Solar Energy Materials & Solar Cells 161 (2017) 247–254

Contents lists available at ScienceDirect

Solar Energy Materials & Solar Cells

journal homepage: www.elsevier.com/locate/solmat

Photothermal effect on Fe_3O_4 nanoparticles irradiated by white-light for energy-efficient window applications

Yuan Zhao[a], M.E. Sadat[b], Andrew Dunn[a], Hong Xu[c], Chien-Hung Chen[d], Wagner Nakasuga[d], Rodney C. Ewing[d], Donglu Shi[a,*]

[a] The Materials Science and Engineering Program, Department of Mechanical and Materials Engineering, College of Engineering and Applied Science, University of Cincinnati, Cincinnati, OH 45221, USA
[b] Department of Physics, University of Cincinnati, Cincinnati, OH 45221, USA
[c] Med-X Institute, Shanghai Jiao Tong University, Shanghai 200030, PR China
[d] Department of Geological Sciences, Stanford University, Stanford, CA 94305-2115, USA

ARTICLE INFO

Keywords:
White-light
Photothermal effect
Fe_3O_4
Thin film
U-factor

ABSTRACT

A significant energy loss results from the poor thermal insulations of the commercial and public buildings. Windows diffuse a large fraction of building heating and cooling energy to the external environment, representing an annual impact of 4.1 quadrillion British thermal unit of primary energy in the US. The current technology for efficient windows relies upon the double-pane insulated glass unit with an insulating gas in between. A key challenge is to reduce thermal conductivity of the windows without relying on insulating materials. The photothermal effect can be possibly utilized for particular functionalities that can collect solar energy for reducing heat loss. The insulation efficiency is quantified through the U-factor, defined as the ratio of the heat flux (*H)* per unit area through the pane to the difference (ΔT) between the window interior surface and exterior temperatures. Upon solar irradiation, single-panes can "self-heat" *via* the photothermal effect from the nanoparticle coatings. This can effectively reduce ΔT for enhanced thermal insulation. In this study, the photothermal effect on Fe_3O_4 nanoparticles stimulated by solar light was investigated for nanoparticles in solutions and as thin films for energy–efficient windows. The Fe_3O_4 nanoparticles were surface-functionalized with different polymers to modulate colloidal stability and for the investigation of the photothermal effect. The photothermal heating efficiencies of Fe_3O_4 with different surface coatings were found to be much greater under the white-light irradiation than near infrared (NIR) in both aqueous suspension and as thin films. The mechanism for the photothermal effect of Fe_3O_4 was identified in terms of its band structure. Both Urbach energy and band gap were obtained based on absorption spectra of various Fe_3O_4 nanoparticles. The Urbach "tail" was found consistent with nanoparticle surface defect structures, while the band gap (~3.1 eV) corresponded to the electronic transitions in the octahedral site of Fe_3O_4. We also discuss the absorption-based photonic physics responsible for the much-enhanced photothermal heating by white-light as compared with NIR. Based on the photothermal heating, the U-factors were obtained with the nanoparticle coatings that show promise in producing energy efficient windows.

1. Introduction

The heating and cooling cycle of commercial and residential buildings represents a significant amount of energy loss [1]. One of the major heat losses is through windows, which is characterized by the so-called U-factor. U-factor is defined as the ratio of the heat flux (H) per unit area through the pane to the difference (ΔT) between the interior and exterior temperatures, as schematically depicted in Fig. 1 [2]. Lower U-factors corresponds to the better insulating windows. The U-factor for an entire window needs to be less than 0.30 Btu/ft²·°F h (1.7 W/m^2 K) to achieve Energy Star certification in the U.S. colder regions [3]. Under extremely cold conditions, the ΔT of a single pane window causes a significant heat loss. The current technology for efficient windows relies upon the double-pane or even triple-pane insulated glass unit with a low-emissivity coating. Although these units may meet some of the requirements in building energy efficiency, the high cost in their manufacture and implementation to replace the existing windows can be prohibitive. Thus, the key challenge is to

* Corresponding author.
E-mail address: Shid@ucmail.uc.edu (D. Shi).

http://dx.doi.org/10.1016/j.solmat.2016.11.039
Received 12 September 2016; Received in revised form 8 November 2016; Accepted 27 November 2016
Available online 09 December 2016
0927-0248/

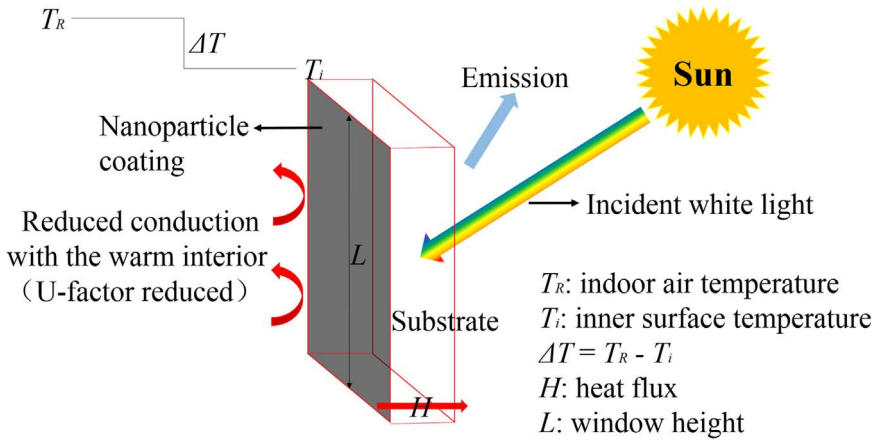

Fig. 1. Schematic diagram showing the concept of U-factor reduction *via* the photothermal effect of the Fe_3O_4 nanoparticle coating on single-pane.

develop a simple but effective technique built upon the existing windowpanes. A straightforward approach would be if these single panes could be coated by a low-cost "self-heating" thin film when exposed to solar light. Upon raising the window surface temperature, the U-factor can be effectively lowered, leading to much reduced heat loss.

The photothermal effects [4–7] of nanoparticles, such as gold [6,8–10], graphene [11], and Fe_3O_4 [4–6], by near-infrared (NIR) irradiation have been extensively investigated. These nanoparticles all exhibit strong NIR-induced photothermal effects, raising the solution temperature by more than 30 °C. Preliminary results show that, upon NIR-laser irradiation, the temperature of the Fe_3O_4 nanoparticle aqueous suspensions increases within short periods, from room temperature to 45 °C [4]. All of these previous photothermal effect studies used NIR radiation (~800 nm) for the biomedical applications [4–7]. However, the photothermal effect induced by white-light has never been investigated for Fe_3O_4 in energy applications. Specifically, the photothermal effect mechanism induced by white-light is not understood in terms of the band structure of Fe_3O_4. The energy conversion mechanism has been extensively studied for gold nanoparticles based on localized surface plasmon resonance (LSPR) [6]. LSPR may apply to noble metals due to their high charge densities. But LSPR may not be majorly responsible for the photothermal effect in Fe_3O_4, which has limited charge carriers.

The goal of this study was to investigate the photothermal effects of Fe_3O_4 nanoparticles in both solution and thin film forms using simulated-solar light. By solar irradiation of nanoparticle coatings on glass substrates, photothermal heating was generated to control ΔT, based on which the U-factor was lowered for energy-efficient windows. Furthermore, the photonic physics was studied that underlies the photothermal effect of Fe_3O_4 nanoparticles induced by white-light irradiation. The relation between the electronic band and nanostructure was established, under white light irradiation, for the newly discovered photothermal effect of Fe_3O_4 nanoparticles. Photon absorption was analyzed and correlated to heat conversion of the Fe_3O_4 nanoparticles with different defect structures.

2. Experimental results

In order to perform photothermal heating measurements, both the liquid and thin film samples were irradiated by 0.1 W/cm^2 white light using a Newport 150 W solar simulator (Lamp model 67005). The experimental apparatus of the white-light mediated photothermal heating system is shown in Fig. 2a. For laser photothermal experiment (the apparatus is shown in Fig. 2b), the light source is a 785 nm laser generator (FC-785-5W-MM Fiber Output Laser System, SFOLT Co., Ltd.). As shown in the Fig. 2, the temperature is recorded by an AVIO G100EXD infrared thermal camera. Light is turned on for a given

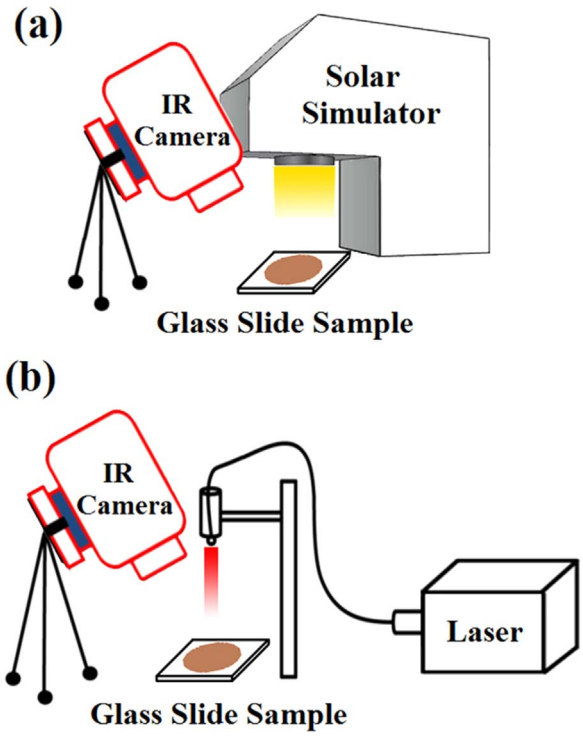

Fig. 2. (a) Apparatus for the photothermal heating experiment using white-light and (b) Apparatus for the photothermal heating experiment by NIR laser.

period of time, and then off but with thermal camera still recording the temperature during the continuous heating experiments. All experiments were performed at room temperature.

Fig. 3 shows the high magnification transmission election microscopy (TEM) images of Fe_3O_4 nanoparticles. As can be seen from Fig. 3a Uncoated Fe_3O_4 particles contain approximately 10 nm diameter nanoparticles and exhibit quite a clear lattice image with sharp particle surfaces and boundaries. Fig. 3d shows the uncoated Fe3O4 with ~5% weight loss to water evaporation. The poly(acrylic acid) coated Fe_3O_4 (PAA-Fe_3O_4) (Fig. 3b) nanoparticles show, however, ~12% mass loss due to PAA vaporization (Fig. 3e). The polystyrene embedded Fe_3O_4 (PS-Fe_3O_4) (Fig. 3c) is morphologically different from Uncoated Fe_3O_4 and PAA-Fe_3O_4 nanoparticles. As shown in Fig. 3c, the Fe_3O_4 nanoparticles (~10 nm) are in fact embedded in the polystyrene spheres (100–200 nm) with a high polymer volume fraction. TGA shows ~36% mass loss due to polystyrene vaporization (Fig. 3f). This unique morphological characteristic makes, as will be shown later, an

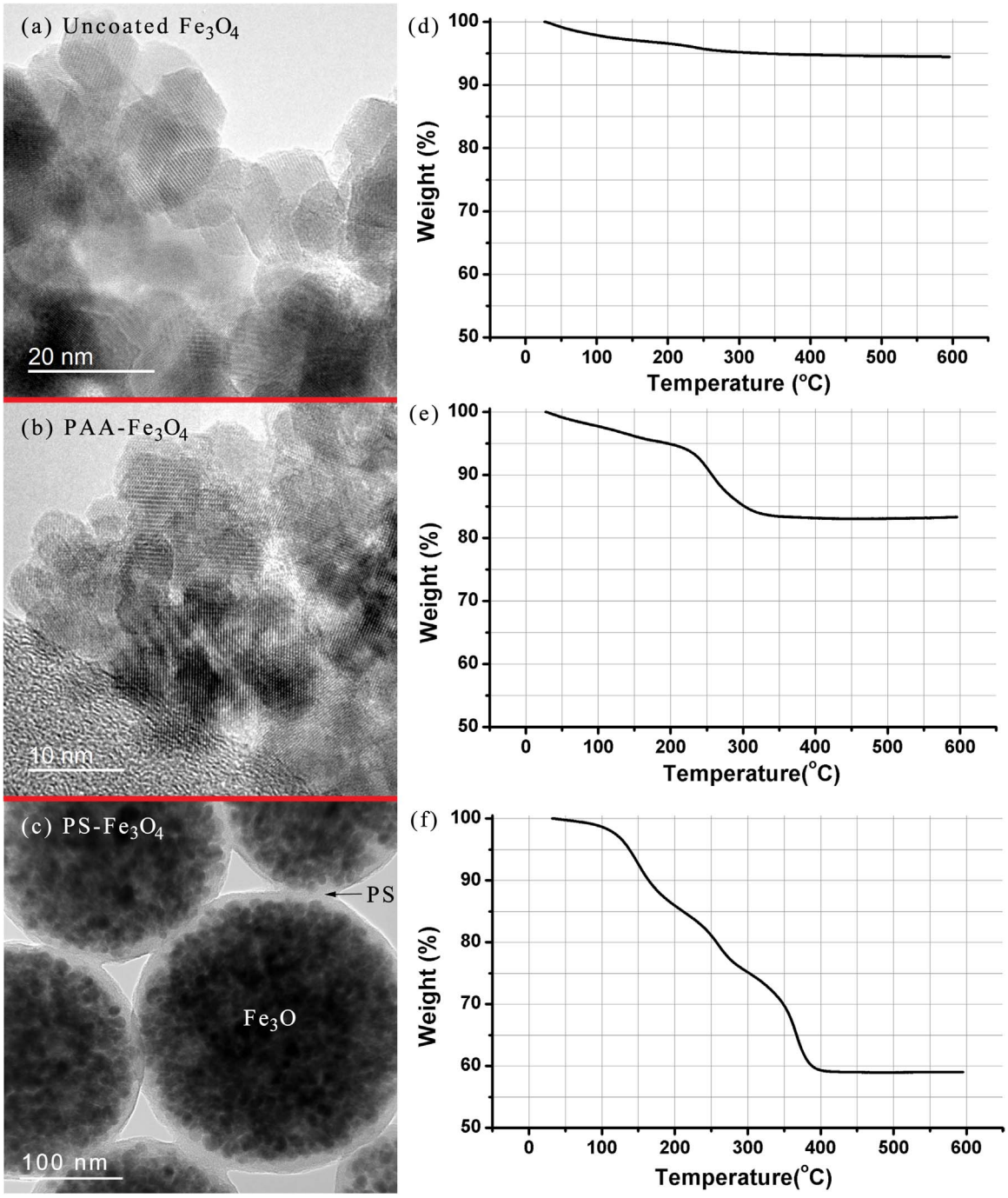

Fig. 3. TEM images of Fe_3O_4 nanoparticles (solutions). (a) Uncoated Fe_3O_4; (b) PAA-Fe_3O_4, and (c) PS-Fe_3O_4. Thermal gravimetric analysis of (d) Uncoated Fe_3O_4 (e) PAA-Fe_3O_4 (f) PS-Fe_3O_4.

important difference in the light absorption behavior.

Fig. 4 shows the surface morphologies of the drop-cast, thin films of Fe_3O_4 on the glass substrates. As can be seen, the thin film surface morphologies consistently reflect the different surface treatments of the Fe_3O_4 nanoparticles. As shown in Fig. 4a, the Uncoated Fe_3O_4 exhibits a rather rough surface due to poor dispersion in the solution. In contrast, the thin films with PAA-Fe_3O_4 (Fig. 4b) nanoparticles show smooth surfaces as a result of good dispersion associated with surface functionalization. The thin film surface morphology shown in Fig. 4c is consistent with that of PS-Fe_3O_4 (Fig. 3c). As the Fe_3O_4 nanoparticles are embedded in the polystyrene spheres. The small clusters in the thin film are evident (Fig. 4c).

Fig. 5 shows the time dependent temperature curve of PAA-Fe_3O_4 solution at various concentrations (0.25, 0.5 and 1.0) mg mL^{-1}. In order to investigate the photothermal effect each sample is illuminated with the white-light using the solar simulator at the light intensity of 0.1 W/cm^2, which is approximately the same radiation density at the surface of Earth from the sun. All samples exhibit the photothermal effect (Fig. 5a); however, the magnitude depends on the Fe_3O_4 concentration, as expected. Under irradiation of white-light with only a low intensity of 0.1 W/cm^2, the temperature of the 1.0 mg mL^{-1} sample increases from 24 °C to 35 °C within 15 min, a temperature increase of 11 °C. Even for a low concentration, 0.25 mg mL^{-1}, within the same time period (15 min), the temperature rises to 32 °C, indicating a significant photothermal effect. After 15 min of exposure to white-light, the samples were allowed to cool to room temperature

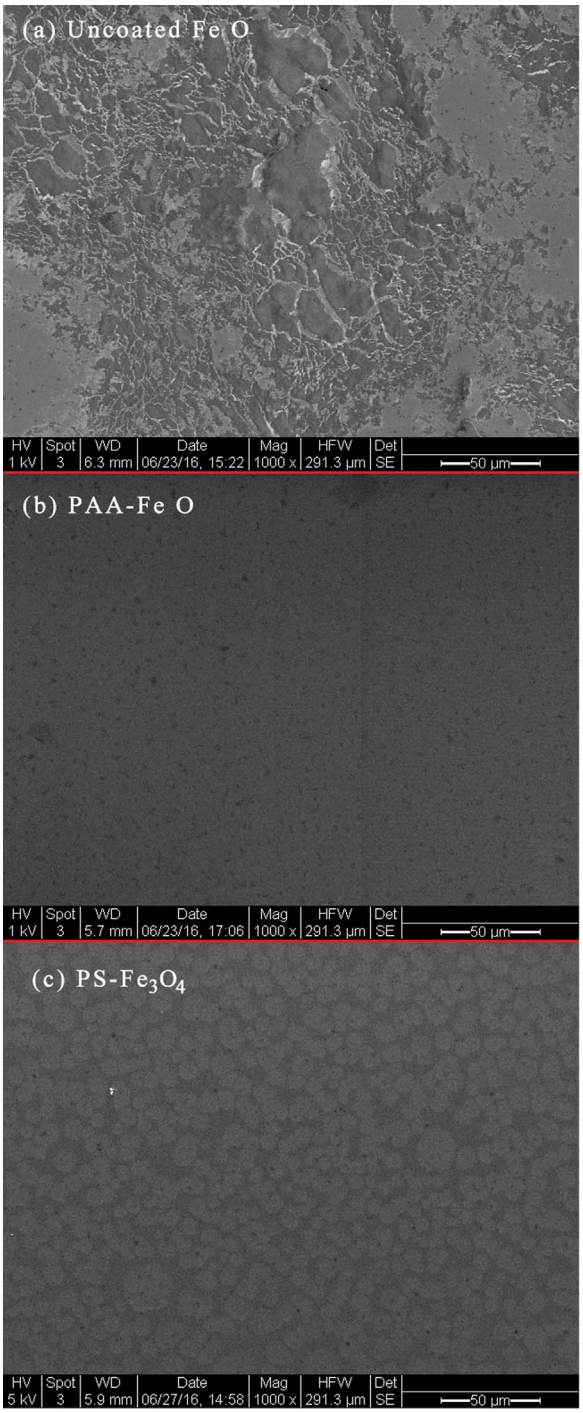

Fig. 4. SEM images of slide samples. (a) Uncoated Fe_3O_4; (b) PAA-Fe_3O_4, and (c) PS-Fe_3O_4.

for 10 min after the white-light was turned off. All samples exhibited approximately the same cooling rates indicating their heat losses to the surroundings are consistently similar.

For comparison, we investigated the photothermal effect of the same PAA-Fe_3O_4 nanoparticle solutions under 785 nm near infra-red (NIR) laser irradiation, at the same light intensity of 0.1 W/cm^2. As shown in Fig. 5b, the 785 nm NIR laser generates a much lower level of heating than the white-light at the same concentration of 1.0 mg mL^{-1}, where temperature increased slightly from ~23.5–27 °C, a temperature gain of 3.5 °C within 15 min. Much weaker photothermal heating is evident in Fig. 5b for the 0.25 mg mL^{-1} sample with only a small increase in temperature. These results show the higher efficiency of the

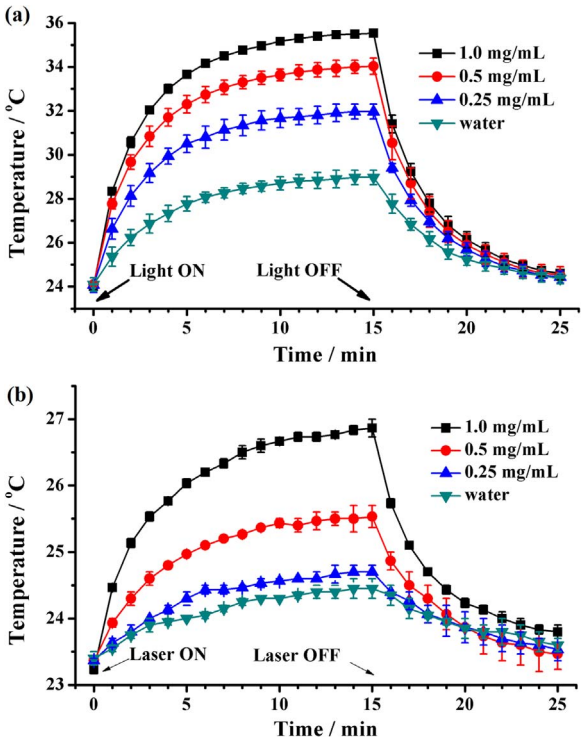

Fig. 5. (a) Temperature *vs.* time curve for the different concentrations of PAA-Fe_3O_4 solutions under white-light. Intensity of the illuminated light: 0.1 W/cm^2; (b) Temperature *vs.* time curve of the different concentrations of PAA-Fe_3O_4 solutions under 785 nm laser. Intensity: 0.1 W/cm^2.

white-light irradiation as compared with NIR, in generating the photothermal heat in the Fe_3O_4 nanoparticles. It is important to note the heating rates under both types of irradiations. It is obvious from both Fig. 5a and b that the initial heating rate under white-light is more rapid than that of the laser heating.

We also investigated the photothermal effect of the thin film samples on a glass substrate, under the same light intensity, namely, white-light and NIR. The thin film samples contained Fe_3O_4 particles with different surface coatings. Fig. 6a shows the time dependent temperature curves of the thin films for different types of nanoparticles. There is a total of 3 mg of Fe_3O_4 on each glass slide for all samples. At the white-light irradiation with an intensity of 0.1 W/cm^2, as shown in this figure, the Uncoated Fe_3O_4 sample experiences an increase in temperature from 25.5 °C, to 33 °C, while the PAA-Fe_3O_4 sample heats to 31.5 °C, even more rapidly. The PS-Fe_3O_4 samples are less efficient, resulting in a temperature rise to less than 30 °C. A common heating behavior of these thin film samples is an initial rapid rise in temperature within minutes, reaching a plateau of constant temperature. This behavior is quite different from their behavior in solution (Fig. 5a and b), under gradual heating. The water in the aqueous solution acts as a heat reservoir with high heat capacity, causing the maximum temperature (T_{max}) to be reached after a longer period (Δt) compared to the thin film samples.

The response of various Fe_3O_4 thin films were investigated by turning on and off the white-light for specific times. Fig. 6b shows the heating curves of different Fe_3O_4 films irradiated by 0.1 W/cm^2 white light in cycles for the times indicated. The initial white-light exposure was for 15 min, followed by another 15 min exposure after 5 min. This cycle was repeated with each heating period lasting 15 min. The thin film samples, although containing different Fe_3O_4 nanoparticles, are heated rapidly and repeatedly, reaching the maximum temperature within a few minutes.

Fig. 7 shows the absorption and transmission spectra of the thin films containing a variety of Fe_3O_4 nanoparticles (the same as tested

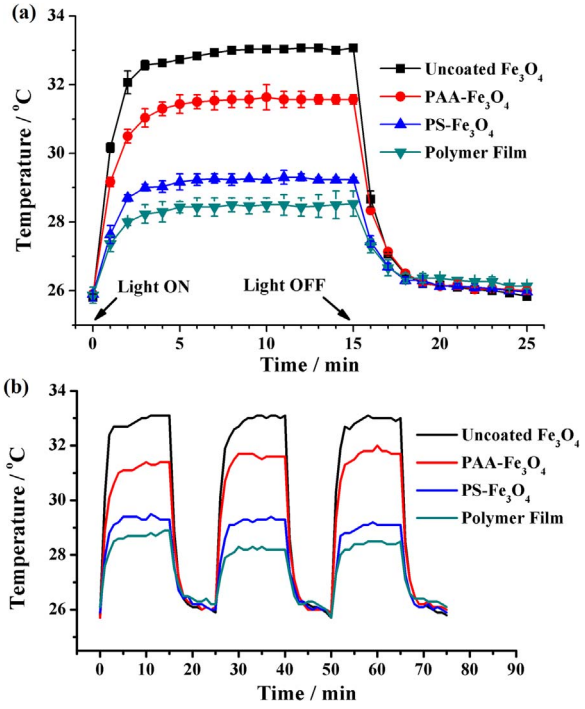

Fig. 6. (a) Temperature *vs.* time for the thin film samples containing various Fe_3O_4 nanoparticles indicated. There is 3 mg Fe_3O_4 per slide. Heating power: 0.1 W/cm^2; (b) Temperature *vs.* time in a cyclic fashion for the thin film samples containing various Fe_3O_4 nanoparticles as indicated. There is 3 mg Fe_3O_4 per slide. Heating power: 0.1 W/cm^2.

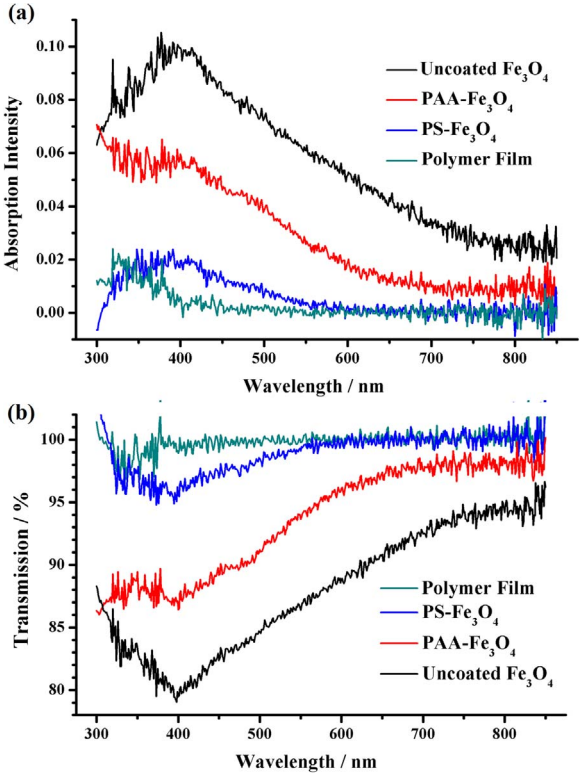

Fig. 7. (a) Absorption *vs.* wavelength for thin samples containing various Fe_3O_4 nanoparticles indicated; (b) Transmission *vs.* wavelength for thin samples containing various Fe_3O_4 nanoparticles indicated.

and shown in Fig. 6a). As can be seen in Fig. 7a, the Uncoated Fe_3O_4 thin film on the glass slide exhibits an absorption peak at 390 nm with the highest absorption and lowest transmission (Fig. 7b). All other thin films containing PAA-Fe_3O_4 and PS-Fe_3O_4 show peaks near 390 nm but at considerably lower absorptions and corresponding transmissions, as expected. The PS-Fe_3O_4 exhibits the lowest absorption, which is consistent with its morphology shown in Fig. 4c. The PS-Fe_3O_4, as reported previously [12], is essentially a polystyrene nanosphere (100–200 nm) with much finer (~10 nm) Fe_3O_4 particles embedded in its polymer matrix. In this case, the polymer matrices reflect most of the incident light, quite similar to the pure polymer control as shown in Fig. 7. The heating behavior observed in Fig. 6 for these samples are consistent with the absorption behavior, where higher absorption of light leads to stronger photothermal effect (or higher overall temperature increase). As expected, Uncoated Fe_3O_4 is more light absorptive than all other samples, therefore exiting the strongest photothermal effect.

3. Discussion

The photothermal effect has been extensively studied for excellent conductors with high charge carrier densities, such as gold and graphene, with the energy conversion attributed to the localized surface plasmon resonance (LSPR) [6,13,14]. A localized plasmon is the result of the confinement of a surface plasmon in a nano particle smaller than the wavelength of the incident light. A nanoparticle's response to the oscillating electric field has been described by the so-called dipole approximation of Mie theory [4]. However, LSPR is unlikely to be the major mechanism for Fe_3O_4 nanoparticles because they lack sufficient charge density.

We have recently investigated the photothermal effect in Fe_3O_4 nanoparticles and explained the process based on the photoluminescence emission in the NIR region [6]. However, the energy conversion mechanism has not yet been well established for Fe_3O_4 nanoparticles under white-light with a continuous spectrum. In Fig. 8, the absorption co-efficient (α) is plotted against photon energy (E) for different types of nanoparticles [15], based on the absorption data shown in Fig. 7. The absorption coefficient α is represented by [14]:

$$\alpha = \alpha_o \exp[\frac{\sigma(E - E_o)}{k_B T}] \quad (1)$$

where α_o is the absorption coefficient, E is the incident energy, and E_o is the onset of absorption. Both α_o and E_o in Eq. (1) are material-dependent constants. $E_u = k_B T/\sigma$ is defined as the Urbach energy (or Urbach "tail"), where σ is the steepness parameter and k_B is the Boltzmann constant. Urbach energy is related to the presence of structural defects, and for the nanoparticles in this study, mostly reflects the functional groups at the surfaces, as each is coated with different polymers. The Urbach tail of the absorption coefficient *vs.* photon energy can be used to characterize the strong internal fields from surface defects. Surface defects on nanoparticles are an important factor that influences the Urbach exponential absorption tail.

According to Eq. (1), we have

$$\ln \alpha = \ln \alpha_0 + \frac{E - E_0}{E_u} \quad (2)$$

Urbach Energy is calculated from the reciprocal of the slope of ln α *vs.* photon energy, taken from the spectra in Fig. 7. By plotting the absorption coefficient on a logarithmic scale as a function of photon energy, the Urbach energy is obtained from the linear portion of the curve (Fig. 8a). Using Eq. (2), the Urbach Energy values of the Uncoated Fe_3O_4 and PAA-Fe_3O_4 were determined to be 0.5245 eV, and 0.6457 eV respectively. These values indicate, consistently, that the surfaces of Fe_3O_4 are effectively modified by PAA functionalization, thus reducing the defect density in PAA-Fe_3O_4, as compared with that of the Uncoated Fe_3O_4. We have analyzed only the Uncoated Fe_3O_4 and PAA-Fe_3O_4 in order to make a direct comparison.

The electronic structures of bulk magnetite (Fe_3O_4) have been

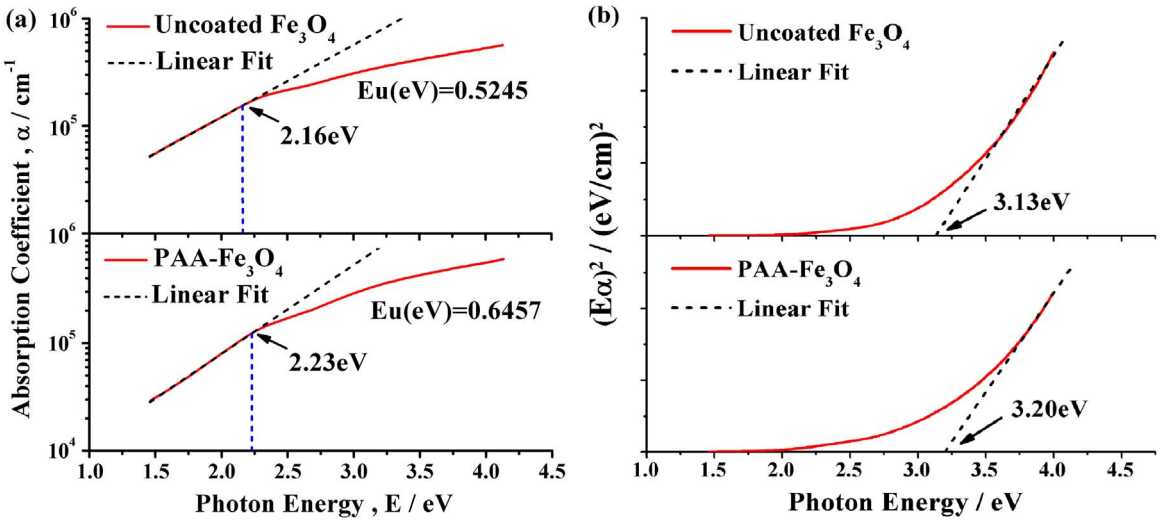

Fig. 8. (a) Absorption coefficient *vs.* photon energy for Uncoated Fe_3O_4 and PAA-Fe_3O_4. (b) $(E\alpha)^2$*vs.* photon energy for Uncoated Fe_3O_4 and PAA-Fe_3O_4.

extensively studied [16,17]. The band gap between the O(2p) and the empty Fe(4s) in Fe_3O_4 is in the range of 4–6 eV [16,17]. The electronic structure is influenced by both the octahedral and tetrahedral sites with the *3d* metal atomic orbital. The energy gap is due to crystal-field splitting on the octahedral site, $\Delta_{cf,o}$–2.2 eV, while that of the tetrahedral site is: $\Delta_{cf,t}$–0.9 eV. The valence band of O(2p) is further split from crystal field site t_{2g}, e of the octahedral and tetrahedral sites, respectively, by almost ~0.9 eV [18,19]. Alvarado et al. have investigated the one electron energy level of Fe_3O_4 in order to describe *3d* photoelectronic excitation using electron spin polarization (ESP), energy distribution curve (EDC), and far-ultraviolet photoelectron spectroscopy measurements [20]. In Alvarado's work, they completed reflection and absorption measurements for a variety of iron oxides including FeO, Fe_3O_4 and Fe_2O_3, and found a similar characteristic spectroscopic signature. Not only was an absorption edge at 2 eV found, several peaks were also resolved at 1.5 eV, 3.2 eV and 5.5 eV [20]. They associated the absorption edge at 2 eV to the optical transition from the last occupied *d* band to the 4s(Fe) band. Balberg & Pankove determined a crystal field splitting value of Δ_{cf} = 1.7 eV, and an exchange splitting Δ_{ex} = 2.7 eV between the majority spin levels (assumed spin down) [21]. Fig. 8b shows the plot of $(E\alpha)^2$ as a function of photon energy, based on which the direct band gap value can be estimated by extrapolation of the linear portion of the curve to the x–axis (Fig. 8b). Using this approach, we have determined the band gap values for the Uncoated Fe_3O_4 (3.08 eV) and PAA-Fe_3O_4 (3.22 eV). These values are consistent with the band gap (~3.1 eV) between O(2p) and (e_g) of the octahedral site.

Fig. 9 shows the extinction (Q_{ext}), absorption (Q_{abs}) and scattering (Q_{sca}) efficiencies as a function of wavelength for PAA-Fe_3O_4 and Uncoated Fe_3O_4 respectively. The values are calculated by the Mie theory using the complex refractive indices of the samples. [5]:

$$Q_{ext} = \frac{2}{x^2}\sum_{n=1}^{\infty}(2n+1)\mathrm{Re}[a_n + b_n] \tag{3}$$

$$Q_{sca} = \frac{2}{x^2}\sum_{n=1}^{\infty}(2n+1)[|a_n|^2 + |b_n|^2] \tag{4}$$

$$Q_{abs} = Q_{ext} - Q_{abs} \tag{5}$$

where a_n and b_n are the coefficients, $x = \frac{2\pi n_{med}\gamma}{\lambda_0}$ is the size parameter with γ being the mean radius of the particles, n_{med} is the refractive index of the media, and λ_o is the vacuum wavelength. Numerical values of Q_{ext}, Q_{abs} and Q_{sca} were calculated as a function of wavelength using the code "Mie-Plot" written by Philip Laven [22]. The extinction coefficient is defined as the imaginary part of the complex index of refraction, which is associated to light absorption. As shown in Fig. 9, the extinction efficiency of Uncoated Fe_3O_4 is considerably higher than that of PAA-Fe_3O_4 over the entire spectrum, which is consistent with the absorption spectra shown in Fig. 7. The absorption efficiency of the Uncoated Fe_3O_4 remains above 1.0 up to a wavelength of 550 nm, while that of PAA-Fe_3O_4 drops rapidly below this value above 400 nm (Fig. 9). The scattering efficiency of the Uncoated Fe_3O_4 is also greater

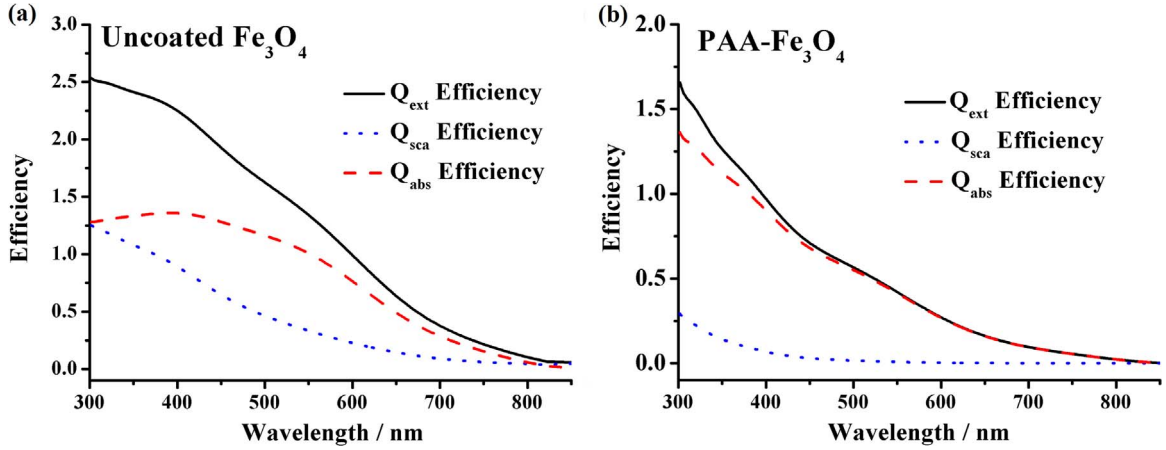

Fig. 9. Extinction (Q_{ext}), absorption (Q_{abs}), scattering (Q_{sca}) efficiencies as a function of wavelength for Uncoated Fe_3O_4 and PAA-Fe_3O_4 respectively.

than that of PAA-Fe_3O_4 due to a difference in their hydrodynamic size (PAA-Fe_3O_4: 66.69 nm±21.56 nm and Uncoated Fe_3O_4: 277.8 nm±97.6 nm; measured by Malvern Zetasizer Nano Series). Even though the core Fe_3O_4 particle diameters of both Uncoated Fe_3O_4 and PAA-Fe_3O_4 are approximately the same (~12 nm), hydrodynamic diameter of Uncoated Fe_3O_4 is significantly larger than PAA-Fe_3O_4 due to severe agglomeration of Uncoated Fe_3O_4. In Mie scattering, the light intensity distribution pattern varies with the particle size. As the particle size decreases, the pattern of the diffracted and scattered light spreads away from the forward direction. Although in the data shown in Fig. 7 there is an overall absorption, the effect of size on scattering efficiency is rather pronounced (Fig. 9). The larger clusters of Uncoated Fe_3O_4 result in a greater scattering efficiency.

Photoluminescence (PL) measurements of Fe_3O_4 have been completed by Sadat et al. over a broad size range of (10 nm–5 μm) [5]. They found three major PL peaks near 540 nm, 690 nm and 840 nm, when illuminated with 407 (3.05 eV) nm laser light for PAA-Fe_3O_4 (the same material used in this study). Similar PL spectra were obtained using the excitation light of 449 nm (2.76 eV). The PL emission exhibits two major peaks at 550 nm (2.10 eV) and 674 nm (1.84 eV) for PAA-Fe_3O_4, whereas for Uncoated Fe_3O_4, PL degradation is observed (Fig. 10), and there is only one peak at 674 nm (1.84 eV). The hydrophilic PAA-coated nanoparticles tend to have higher PL due to water molecules in a gas phase perform good passivation of the dangling bonds at the iron-oxide interface. Similar results have been presented by Gongalsky et al. [23]. According to the study by Sadat et al. [5], the PL peak near 550 nm (2.30 eV) is attributed to the radiative recombination of mobile electrons from $t_{2g} \rightarrow e_g$(2.2 eV) on the octahedral site. The much weaker peak at ~690 nm (1.79 eV) corresponds to the recombination of trapped electrons from the octahedral site to O(2p) on tetrahedral site. Sadat *et al.* found that, under 808 nm laser irradiation, the extinction efficiency of PAA-Fe_3O_4, calculated by the Mie theory, is mostly absorption dominated [5]. However, as shown in Fig. 7a, the absorption in the NIR range is very much reduced. The absorption of the Uncoated Fe_3O_4 peaks at 410 nm with the maximum intensity on the scale of 10 while that has decreased to the scale of 3 in the NIR range above 800 nm.

The wavelength of 410 nm corresponds to a photon energy of 3.02 eV, precisely the gap width between O(2p) and (e_g) of the octahedral site. Other Fe_3O_4 nanoparticles such as PS-Fe_3O_4 and PAA-Fe_3O_4 exhibit the same absorption peaks near 410 nm. These results indicate that the most absorption takes place at the incident photon energy comparable to the energy gap between O(2p) and (e_g) of the octahedral site. Photon energies away from this value (~3.0 eV) may contribute to absorption but to a much lesser degree, especially in the NIR region. This interpretation is consistent with the photothermal effect results shown in Fig. 5a and b. For the same concentration of PAA-Fe_3O_4 solution, irradiation by white-light results in a much stronger photothermal effect because the incident light spectrum contains the photon energy (410 nm, 3.02 eV), which is on the same order of magnitude as the Fe_3O_4 energy gap (3.1 eV). Thus, absorption is the highest at this wavelength (410 nm) (Fig. 7a). The strong absorption at 410 nm explains as to why the photothermal heating is much more prominent under white-light irradiation as compared with NIR.

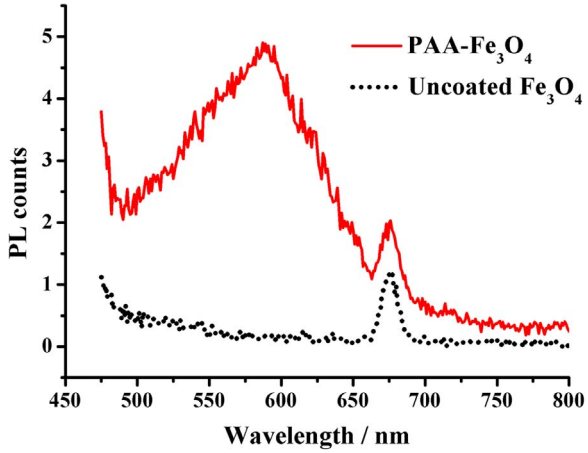

Fig. 10. Photoluminescence *vs.* wavelength for the Fe_3O_4 nanoparticles indicated.

The results of photothermal heating of various thin films shown in Fig. 6a are consistent with the absorption data (Fig. 7a). The thin film containing Uncoated Fe_3O_4 exhibits the highest heating rate and reaches the maximum within a few minutes. As expected, Uncoated Fe_3O_4 also exhibits the strongest light absorption (Fig. 7a). The degree to which the light is absorbed depends on the polymer to Fe_3O_4 ratio. Quite consistently, the PS-Fe_3O_4 has higher polymer content, therefore the less absorption (similar with the polymer control). As reported previously [12], PS-Fe_3O_4 is essentially a polystyrene nanosphere with fine Fe_3O_4 nanoparticles embedded in its polymeric matrix. In contrast, PAA-Fe_3O_4 has much lower polymer to Fe_3O_4 ratio, and shows a considerably higher absorption and photothermal heating (Fig. 6a).

U-Factor is a measure of thermal transport through conduction, convection, and radiation. In the United States, the National Fenestration Rating Council (NFRC) implements a national rating system for energy performance of fenestration products, and NFRC has standardized the environmental conditions for U-factor calculations as following equation [24]:

$$U = \frac{1}{1/h_h + 1/h_c + 1/U_L} \tag{6}$$

where h_h and h_c are the interior and exterior heat film coefficients respectively, and U_L is the heat transfer coefficient of the windowpane assembly alone without indoor and outdoor air film coefficients. h_h can be calculated using the following equations [24]:

$$h_h = 1.46 \times \left(\frac{\Delta T}{L}\right)^{0.25} + \sigma e\left[\frac{T_R^4 - (\Delta T)^4}{\Delta T}\right] \tag{7}$$

where L is the total height of a window, σ is the Stefan–Boltzmann constant (5.67×10^{-8} W/m^2 K^4), e is the emissivity, T_R is the indoor air temperature, and ΔT is the temperature difference between window inner surface and indoor air, as schematically shown in Fig. 1.

The outside heat film coefficient h_c is usually calculated through the air (wind) velocity by Lokmanhekim's method [25]:

$$h_c = 8.07 \times v^{0.605} (v > 2m/s) \tag{8}$$

Assuming steady-state condition, homogeneous temperature variables, and neglecting edge and radiation effects, U_L can be derived from h_h [26]:

$$1/U_L = R_L \tag{9}$$

where R_L is the resistance of the windowpane assembly alone.

Using the Eqs. (6)–(9), U can be expressed as:

$$U = \frac{1}{\frac{1}{8.07 \times v^{0.605}} + \frac{1}{1.46 \times \left(\frac{\Delta T}{L}\right)^{0.25} + \sigma e\left[\frac{T_R^4 - (\Delta T)^4}{\Delta T}\right]} + R_L} \tag{10}$$

Under the aforementioned NFRC standards (interior air temperature:21.1 °C, exterior air temperature: −17.8 °C, wind speed:12.3 km/h, window height 1.524 m) of measuring the center-of-glass U-factor, we used the Eq. (10) to analyze the possible impacts of temperature difference ΔT on the center-of-glass U-factor. If we select 1.8 mm organoclay nanolaminate as the possible dense solid insulating material, the R_L is 0.22 W/m^2 K and the emissivity is 0.30, as literature reported [27,28]. According to Fig. 6, PAA-Fe_3O_4 thin film increased approximately 5 °C after white light irradiation. If we assume the real products have the same performance, hence a similar ΔT as

observed under experimental conditions, the U-factor reduces 0.08–0.15 W/m^2 K as the U-factor is dependent on the initial surface temperature of the heating glass. This corresponds to an energy savings of 85–159 KJ/m^2 in one-hour white light irradiation based upon aforementioned assumptions.

4. Conclusions

We have investigated the photothermal effects of various Fe_3O_4 nanoparticles in both solution and thin film forms under white-light and NIR laser irradiation. Much stronger photothermal effect is found for Fe_3O_4 under white-light irradiation as compared with the NIR laser irradiation. The significantly enhanced photothermal heating under white-light is explained by the electronic structure of Fe_3O_4. The strongest absorption takes place near 410 nm, which corresponds to the energy gap of Fe_3O_4 caused by crystal-field splitting on the octahedral site. Nanoparticle surface polymer coatings alter photon absorption; therefore, lower the photothermal heating efficiency. With sufficient photothermal effect under white light irradiation, the U-factor can be effective lowered, leading to reduced heat loss. The solar-induced photothermal effect will have promise in energy applications, especially in making energy sufficient windows.

5. Experimental details

The Fe_3O_4 nanoparticles were synthesized with procedures reported previously [29–32]. $FeCl_3{\cdot}6H_2O$ (1.11 g) and $FeCl_2{\cdot}4H_2O$ (0.433 g) were dissolved in distilled H_2O (80 mL) at 70 °C in a Nitrogen environment. After 60 min, NaOH (20 mL) was added to the mixture. The mixture was stirred at 90 °C for another 2 h in a Nitrogen environment. The resulted particles were magnetically separated and washed repeatedly with deionized water until reaching pH value of 7. The final Uncoated Fe_3O_4 nanoparticle solution was 5 mg mL^{-1}. For dispersion purposes, the Fe_3O_4 nanoparticles were coated with various polymers. They are denoted as the Uncoated Fe_3O_4 and PAA-Fe_3O_4, with the prefix indicating the surface-coated polymers, for example, PAA: poly(acrylic acid). The PS-Fe_3O_4, as reported before [29], is essentially the nano-size Fe_3O_4 particles embedded in the matrices of the polystyrene nanospheres (100–200 nm diameter).

Both the liquid and thin film samples were prepared for the photothermal experiments. Fe_3O_4 nanoparticle solutions (0.15 mL) in different concentrations (0.25, 0.5, 1.0 mg mL^{-1}) were added into a 48-well plate. For the thin film sample, 25×25 mm^2 glass slide substrates were sonicated in acetone for 15 min, and dried at 50 °C for 20 min 10% PAA-water solution was diluted from the 40% poly(acrylic acid, sodium salt) solution as the control sample. Fe_3O_4 nanoparticles (3 mg), was added into 40% PAA solution (2.5 mL). Deionized water was added to make each of the 10 mL coating solutions. The coating solutions were shaken overnight for uniformity. Glass slides were coated by coating solution (0.3 mL) through drop casting. During the coating process, the solution was carefully dropped on the center of a glass slide (25×25 mm^2). Then the glass slides were heated by a hot plate at 50 °C for about 20 min to accelerate the evaporation of water to make thin films.

Acknowledgments

We acknowledge the financial support from the National Science Foundation Grants CMMI-1635089 and EEC-1343568. We thank Dr. Andrew Steckel for the use of the Perkin-Elmer spectrophotometer.

Appendix A. Supporting information

Supplementary data associated with this article can be found in the online version at doi:10.1016/j.solmat.2016.11.039.

References

[1] D. Arasteh, S. Selkowitz, J. Apte, M. LaFrance, ACEEE Summer Study on Energy Efficiency in Buildings, Zero energy windows, Pacific Grove, CA, 08, 2006
[2] J. Carmody, Residential Windows: A Guide to New Technologies and Energy Performance, W.W. Norton, New York, 2007.
[3] Environmental Protection Agency, Energy Star performance criteria for windows, doors, and skylights, ⟨https://www.energystar.gov/sites/default/files/Windows_Doors_and_Skylights_Program_Requirements%20v6.pdf⟩, (accessed 08.16).
[4] M. Chu, Y. Shao, J. Peng, X. Dai, H. Li, Q. Wu, D. Shi, Biomaterials 34 (2013) 16.
[5] M.E. Sadat, M. Kaveh Baghbador, A.W. Dunn, H.P. Wagner, R.C. Ewing, J. Zhang, H. Xu, G.M. Pauletti, D.B. Mast, D. Shi, Appl. Phys. Lett. 105 (2014) 9.
[6] H. Yang, H. Liu, M. Li, I. Hsi, C. Fan, C. Huang, Y. Lu, M. Hua, H. Chou, J. Liaw, C.M. Ma, K. Wei, Biomaterials 34 (2013) 22.
[7] D. Shi, Adv. Funct. Mater. 19 (2009) 21.
[8] X. Huang, I.H. El-Sayed, W. Qian, M.A. El-Sayed, J. Am. Chem. Soc. 128 (2006) 6.
[9] P. Huang, L. Bao, C. Zhang, J. Lin, T. Luo, D. Yang, M. He, Z. Li, G. Gao, B. Gao, S. Fu, D. Cui, Biomaterials 32 (2011) 36.
[10] S.H. Tsao, D. Wan, Y. Lai, H. Chang, C. Yu, K. Lin, H. Chen, ACS Nano 9 (2015) 12.
[11] L. Feng, L. Wu, X. Qu, Adv. Mater. 25 (2013) 2.
[12] H. Xu, L. Cui, N. Tong, H. Gu, J. Am. Chem. Soc. 128 (2006) 49.
[13] J. Wang, Z. Zhu, A. Munir, H.S. Zhou, Talanta 84 (2011) 783.
[14] S. Franzen, J. Phys. Chem. C 112 (2008) 15.
[15] T.W. Odom, C.L. Nehl, ACS Nano 2 (2008) 4.
[16] J. Allen, J. Zaanen, G. Sawatzky, Phys. Rev. Lett. 55 (1985) 4.
[17] D.L. Camphausen, Phys. Rev. Lett. 10 (1972) 657.
[18] C. Boxall, G. Kelsall, Z. Zhang, J. Chem. Soc. Faraday Trans. 92 (1996) 5.
[19] v.d. Zaag PJ, W.W. Fontijn, R.R. Metselaar, L. Fiener, M. Devillers, J. Appl. Phys. 85 (1999) 8.
[20] S.F. Alvarado, M. Erbudak, P. Munz, Physica B C 86 (1977) 1188.
[21] I. Balberg, J.I. Pankove, Phys. Rev. Lett. 27 (1971) 20.
[22] P.Laven, MiePlot, ⟨http://www.philiplaven.com/mieplot.htm⟩, (accessed 10.15).
[23] M.B. Gongalsky, A.Y. Kharin, L.A. Osminkina, V.Y. Timoshenko, J. Jeong, H. Lee, B.H. Chung, Nanoscale Res. Lett. 7 (2012) 1.
[24] NFRC 102, Procedure for Measuring the Steady-State Thermal Transmittance of Fenestration Systems, Silver Spring, MD: National Fenestration Rating Council, Inc., Maryland, 2010.
[25] M. Lokmanhekim, Procedure for Determining Heating and Cooling Loads for Computerized Energy Calculations: algorithms for Building Heat Transfer Sub Routines, ASHRAE, New York, 1971.
[26] K. Varshney, J.E. Rosa, I. Shapiro, Int J. Green. Energy 9 (2012) 3.
[27] M.D. Losego, I.P. Blitz, R.A. Vaia, D.G. Cahill, P.V. Braun, Nano Lett. 13 (2013) 5.
[28] F. Giovannetti, S. Föste, N. Ehrmann, G. Rockendorf, Sol. Energy 104 (2014) 52.
[29] D. Shi, H.S. Cho, Y. Chen, H. Xu, H. Gu, J. Lian, W. Wang, G. Liu, C. Huth, L. Wang, R.C. Ewing, S. Budko, G.M. Pauletti, Z. Dong, Adv. Mater. 21 (2009) 21.
[30] H. Cho, Z. Dong, G.M. Pauletti, J. Zhang, H. Xu, H. Gu, L. Wang, R.C. Ewing, C. Huth, F. Wang, D. Shi, ACS Nano 9 (2010) 4.
[31] F. Wang, G.M. Pauletti, J. Wang, J. Zhang, R.C. Ewing, Y. Wang, D. Shi, Adv. Mater. 25 (2013) 25.
[32] D. Shi, N.M. Bedford, H. Cho, Small 7 (2011) 18.